

A general method for impact dynamic analysis of a planar multi-body system with a rolling ball bearing joint

Li-xin Xu

Received: 31 December 2013 / Accepted: 22 May 2014 / Published online: 25 June 2014
© Springer Science+Business Media Dordrecht 2014

Abstract Impact affects the dynamic characteristics of mechanical multi-body systems and damages those rotating parts, such as the joint rolling element bearings, which are high-precision, defect intolerant components. Based on multi-body dynamic theory, Hertzian contact theory, and a continuous contact model, this study proposed a modelling method that can describe the dynamic behaviour of planar mechanical multi-body systems containing a rolling ball bearing joint under impact. In this method, the rigid bodies and bearing joint were connected according to their joint force constraints; the impact constraint between the multi-body system and the target rigid body was constructed using a continuous contact force model. Based on this method, the reflection relationship between the external impacts of the mechanical multi-body system and the variation law governing the dynamic load on the rolling bearing joint were revealed. Subsequently, an impact multi-body system, which was composed of a sliding–crank mechanism containing a rolling ball bearing joint and the target rigid body with an elastic support, was analysed to explore the dynamic response of such a complex discontinuous dynamic system and the relevant relationship governing the dynamic load on the

rolling bearing joint. In addition, a multi-body dynamic simulation software was used to build a virtual prototype of the impact slider–crank system. Compared with the theoretical model, the prototype had an additional deep groove ball bearing. That is to say, the prototype model took account of the specific geometric structural characteristics and the complex contact relationship of the inner and outer races, rolling balls, and bearing cage. Finally, the effectiveness of the theoretical method proposed in this study was verified by comparative analysis of the results. The results suggested that the external impact of a mechanical multi-body system was prone to induce sudden changes in the equivalent reaction force on its bearing joint and the dynamic load carried on its rolling balls. This study provided an effective method for exploring the distribution characteristics of dynamic loads on rolling ball bearing joints under working impact load conditions. Moreover, it offered support for the parameter optimisation of geometric structure, performance evaluation, and dynamic design of the rolling ball bearings.

Keywords Multi-body dynamics · Impact dynamics · Ball bearing · Slider–crank mechanism

L. Xu (✉)
School of Mechanical Engineering, Tianjin University
of Technology and Education, Tianjin 300222, China
e-mail: xulixin_tju@aliyun.com

L. Xu
School of Mechanical Engineering,
Tianjin University, Tianjin 300072, China

1 Introduction

In recent years, the impact dynamics of mechanical multi-body systems have been oft researched. With

regards the dynamic modelling of impact between objects, Zhen and Liu [1] presented a systematic theory for analysing 3-D impact with friction in multi-body systems. Their method can deal with the complex motions appearing in impact such as slip, stick, and slip resumption. Najafabadi et al. [2] proposed a novel approach to the modelling and analysis of impact involving multi-body systems. Their approach is based on a decomposition of the kinetic energy of a unilaterally constrained multi-body system. Bhalerao and Anderson [3] introduced a recursive scheme for flexible multi-body systems involving intermittent contact resulting in a minimal size linear complementarity problem (LCP) at logarithmic cost for parallel implementation. This method is more efficient than other LCP approaches in the presence of bilateral system constraints. Flickinger and Bowling [4] discussed a new dissipation principle for resolving post-impact tangential velocities after simultaneous impact events on a system composed of interconnected rigid bodies. Flores et al. [5] presented a general and comprehensive analysis of continuous contact force models for soft materials in multi-body dynamics. Their approach can be used for contact problems involving materials with low or moderate values of coefficient of restitution. Rodriguez and Bowling [6] proposed a method for determining the post-impact behaviour of a rigid body undergoing multiple, simultaneous impact with friction. In their approach, velocity constraints based on the rigid body assumption were developed and applied to the system equations of motion to make them determinate. Flores et al. [7] presented a method of modelling and analysing contact-impact events in multi-body systems. The effectiveness of the proposed methodology is demonstrated by the dynamic simulation of a cam-follower system on an industrial cutting file machine. The contact impacts followed by rebounds, sliding friction, and stick phenomena were captured in their simulations. For detecting the precise instant of impact in multi-body dynamics, Flores and Ambrósio [8] presented a general method for the automatic detection of precise instant of contact in contact-impact analysis, and for adjusting the integration time-step accordingly. Generally, the calculation of the minimum distance between the surfaces of bodies plays an important role in computational contact-impact mechanics. For this purpose, Lopes et al. [9] proposed a general rigid contact detection method for non-conformal bodies with ellipsoidal and superellipsoidal surfaces. Dopic

et al. [10] applied continuous contact force models to the human-in-the-loop simulation of multi-body systems. Machado et al. [11] presented and discussed several different compliant contact force models used in the context of multi-body system dynamics to model and analyse contact-impact events. To understand more comprehensively the status of research on the impact dynamics of multi-body system, readers can find more details elsewhere [12]. This work appraises the current status of research devoted to the problem of modelling impact in multi-body systems.

As it well known, it is difficult to describe accurately the spatial 3-D collision between contacting objects and reveal the characteristics of the complex dynamic variations in the impact. Therefore, the aforementioned research mainly focuses on impacts between simple objects, such as the collision between a uniform slender rod and a rough fixed surface [1], the impact of a small ball with both ground and wall [6], as well as the collision when a double pendulum freely falls on a rigid plane [4]. Moreover, the effectiveness and correctness of the impact models proposed were proved by numerical simulation analysis. Currently, there is much research regarding the influences of impact on the dynamic response of a constrained multi-body system. In the work to date, planar mechanisms with joint clearance, such as the slider–crank mechanism and the four-bar mechanism were used as research objects to analyse the influences of the impact of the clearance joint on the dynamic response of the attached mechanisms. Ravn [13] proposed a continuous analysis method for the dynamic modelling of planar multi-body systems with joint clearance. The contact force in their clearance joint is calculated by Hertzian contact deformation theory that accounts for the geometrical and material properties of the contacting bodies. A slider–crank mechanism with one clearance joint between the connecting rod and the slider is used as an example. Flores et al. [14] discussed the influence of the clearance and the friction coefficient on the dynamic response of planar rigid multi-body systems. A four-bar mechanism and a slider–crank mechanism are used as examples to demonstrate how a revolute joint with clearance affects the mechanical behaviour. Koshy et al. [15] presented a computational and experimental study of the contact forces developed in revolute clearance joints. It is concluded that the selection of the appropriate contact force model with proper dissipative damping plays a significant role in the dynamic response of mechan-

ical systems involving contact events. However, the above research neglects the effect of lubrication on the dynamic characteristics of a micro-contacting impact in a clearance joint. In real engineering, there is lubricating oil in the joint contact pair that is used to reduce the wear of joint and prolong the service life of the joint. Ravn et al. [16], Schwab et al. [17], Flores et al. [18–20], and Alshaer et al. [21] analysed and compared the dynamic response of a slider–crank mechanism with a dry, and a lubricated, clearance revolute joint, respectively. They each verified that lubrication of the clearance joint can smooth the peak values of the contact forces compared with the unlubricated case. Flores et al. [22] and Machado et al. [23] presented methods for modelling and evaluating the forces produced by a dynamic journal-bearing in a multi-body system. A dynamic simulation of a slider–crank mechanism containing a clearance joint with different radial clearances and oil viscosities verified that a hydrodynamic fluid film journal bearing exhibits a damping effect that plays an important role in the stability of the motion of the system. Tian et al. [24] proposed a novel method for the modelling and analysis of planar flexible multi-body systems with clearance and lubricated revolute joints based on an absolute nodal coordinate method.

In recent years, the rapid development of computer technology made possible the dynamic modelling and highly efficient numerical solution of complex mechanical multi-body systems with multiple clearance joints. Erkaya and Uzmay [25] and Flores and Lankarani [26,27] investigated the dynamic response of a four-bar mechanism and a slider–crank mechanism having two revolute joints with clearance, respectively. Liu et al. [28] and Megahed and Haroun [29] analysed a slider–crank mechanism with one and two clearance joints when working in vertical and horizontal planes. This study shows that, when the mechanism works in the horizontal plane, the rate of impacts at each clearance joint increase and consequently the clearance joints and actuators will deteriorate faster. Muvengei et al. [30] investigated the parametric effects of differently located frictionless revolute clearance joints on the overall dynamic characteristics of a multi-body system. It is observed that different joints in a multi-body system have different sensitivities to the clearance size and the dynamic behaviour of one clearance revolute joint cannot be used as a general case for a mechanical system. More recently, the authors [31]

studied the dynamic behaviour of planar rigid body mechanical systems due to the interaction of multiple revolute clearance joints. It was verified that the clearance joints in a multi-body mechanical system have a strong dynamic interaction. The motion modes including continuous contact, free-flight, and impact in one revolute clearance joint will determine the motion modes in the other clearance joints. For capturing the dynamic behaviour of a multi-body system accurately, all the joints therein should be modelled as clearance joints. Erkaya [32] investigated the effects of joint clearance on the mechanism's trajectory in a walking machine. It is indicated that the mechanism's trajectory is very sensitive to the clearance joint characteristics even if the clearance size is small. Xu and Li [33] discussed the influence of the revolute joint clearances on the dynamic performance of a planar 2-DOF pick-and-place parallel manipulator. The results indicated that the clearance joints present two obvious separation leaps in a complete pick-and-place working cycle of the parallel manipulator, following a collision. The impact induces system vibration and thus reduces the dynamic stability of the system. For improving accuracy in the evaluation of the dynamic behaviour of clearance joints in multi-body systems, Brutti et al. [34] developed a general computer-aided model of a 3-D revolute joint with clearance suitable for implementation in multi-body dynamic solvers. Except for the aforementioned numerical simulations, Erkaya and Uzmay [35] and Flores [36] presented experimental investigations of revolute joint clearance's effects on mechanism dynamic characteristics, respectively. The research on impact dynamics of clearance joint is not limited to planar revolute joints. Tian et al. [37] derived a new approach to model and analyse a spatial flexible multi-body system with a cylindrical clearance joint. In their approach, the misalignment of the journal inside the bearing is studied. Flores et al. [38,39] and Tian et al. [40] presented methods for modelling and simulating both a spatial rigid, and flexible, multi-body system with spherical joints. Furthermore, Flores et al. [41] presented a method for modelling translational joints with clearance in rigid multi-body systems.

Most of the existing research uses the planar multi-body system with revolute joint clearance as its research object to investigate the influences of joint clearance on the dynamic characteristics of system. However, in engineering practice, the rolling element

bearings are often used as revolute joints to connect mechanical components. For example, angular contact bearings used in pairs are key components for the precise transmission of industrial robot joints. Typically, the rolling element bearing is an assembly composed of rolling bodies, a cage, and the inner and the outer races. Therefore, its composition and structure is more complex than a sliding bearing. In addition, in the rotation process of rolling element bearings, there are complex multi-point contacts between rolling bodies, the bearing cage, and the races. All of these determine the complexity of the modelling and solution of the mechanical multi-body system with joint rolling element bearings. In recent years, and with regards the dynamic modelling of rolling element bearings, Jang and Jeong [42–44] presented a non-linear model to analyse the ball bearing vibration due to waviness in a rigid rotor supported by two or more ball bearings. Bai and Xu [45] presented a 5-DOF dynamic model to study the dynamic performance of ball bearings due to the effect of both internal clearance and waviness at high speed, where the centrifugal force and gyroscopic moment from balls were taken into account. Upadhyay et al. [46] developed a mathematical model of a rotor bearing system to observe the non-linear response of an unbalanced rotor. Patel et al. [47] presented a dynamic model for a deep groove ball bearing considering single and multiple defects on the races. Patil et al. [48] modelled a deep groove ball bearing with single and multiple localised defects on inner and outer raceways. Nakhaeinejad and Bryant [49] proposed a detailed model of rolling element bearings with 33-DOF. The effects of type, size, and shape of defects on the vibration response in rolling element bearings were studied. Kappaganthu and Nataraj [50] presented a 2-DOF non-linear model of a rotor-bearing system on rolling element bearings and influence of the bearing asymmetric clearance was considered. Liu et al. [51] proposed a piecewise continuous response function to describe a localised defect of different sizes in a bearing. Kankar et al. [52] investigated the effect of local defects on the stability of a rolling element bearing rotor system. More recently, the present authors [53] proposed a general method for dynamic modelling and analysis of planar multi-body systems containing deep groove ball bearings with clearance. The bearing

joint was modelled by introducing a non-linear constraint force system, which takes into account the contact stiffness interaction between the rolling elements and the raceways. The evaluation of the contact forces was based on Hertzian contact deformation theory that accounts for the geometrical and material properties of the contacting bodies. Later, the dynamic load distribution characteristics of bearings under real multi-body system movement conditions are simulated by the method [54]. By using the approach, we can not only get the variation in the contact load on each ball element in bearing joints with the change of mechanism configuration, but also determine the numbers of balls which bear the load as well as the contact force magnitude.

Basing on multi-body dynamic theory, Hertzian contact theory, and a continuous contact model, this study proposed a modelling method that can describe the impact dynamic behaviour of a planar mechanical multi-body system containing a rolling ball bearing joint. Based on this method, the dynamic characteristics of a rolling ball bearing joint in a multi-body system under impact were revealed. Moreover, we can obtain the equivalent constraint reaction force in the bearing joint and the variation of the dynamic load on each rolling ball in the bearing. This method offers mechanical support for the parameter optimisation of geometric structure, performance evaluation, and dynamic design such joints. The remainder of the paper is organised as follows: Sect. 2 introduces the approach for modelling the impact planar multi-body system with a rolling ball element bearing joint. The content includes methods for modelling the ball bearing joint and the contact constraint in a planar multi-body system, the analysis of the generalised forces in the impact system, and the combination and solution of the equations of motion of the impacted planar multi-body system. In Sect. 3, an impact slider–crank mechanism with a deep groove ball bearing joint is used as a numeral example to verify the method. The variations of the joint reaction force and the dynamic load on each ball element in the bearing are obtained and discussed. Section 4 offers a simulation of the impact slider–crank mechanism as run in MSC.ADAMS software. In the last section, the main conclusions from this study are presented.

2 Dynamic modelling of an impact planar multi-body system with a ball bearing joint

Usually, the rolling element bearing comprises a plurality of rolling elements, uniformly distributed in the inner and outer races of the bearing, and restricted by the cage. During the rolling process of bearing, rolling bodies, the cage, and the inner and outer races of the bearing undergo complex multipoint contact. Moreover, if the influences of the external impact of the multi-body system are taken into consideration, the multi-body system containing the rolling ball element bearing joint is a highly non-linear dynamic system. To reduce the difficulty in building and solving dynamic models of such complex dynamic system, the following assumption was needed:

- (1) The outer and inner races of the bearing are fixedly connected with the bush and journal of the rigid bodies, respectively. With respect to the rigid bodies, there is no rotational degree of freedom for the outer and inner races of the bearing.
- (2) Rolling balls uniformly distribute themselves on the inner and outer races and rotate at the same rate.
- (3) The influence of contact friction between the rolling balls with the inner and outer raceways is neglected.

Figure 1 shows the dynamic model of a multi-body system containing a rolling ball bearing joint under gen-

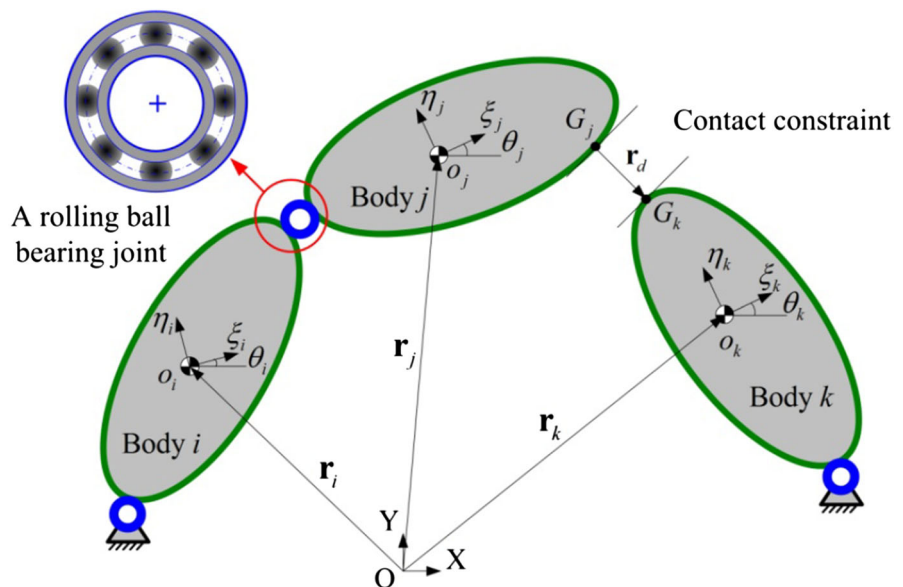
eralised coordinates XOY in a collision. It was assumed that rigid bodies i and j were connected by the joint of the rolling ball bearing; rigid bodies j and k were restricted in collision. G_j and G_k represent the impact contact points between rigid bodies j and k ; \mathbf{r}_d refers to the vector of the relative position of the contact point in the collision. In addition, it was assumed that the body-fixed coordinate system $\xi o \eta$ was located at the centroid of the rigid body. The generalised coordinate \mathbf{q}_i of an arbitrary rigid body in the plane was expressed as:

$$\mathbf{q}_i = [\xi, \eta, \theta]_i^T \tag{1}$$

where, ξ and η are the translational coordinates of the origin in the body-fixed coordinate system; θ denotes the rotational angle of the body-fixed coordinate system versus the generalised coordinate system.

When rigid bodies j and k satisfy the restriction requirements for contact position in the motion of a multi-body system, the interaction of the forces on the contact point is called the impact force. Obviously, external collision forces affect the dynamic response of the system and the distribution characteristics of the dynamic load on the rolling ball bearing joint. To establish the dynamic model for the impacted multi-body system containing a rolling ball bearing joint, two key problems should be solved. First of all, an effective model of the revolute joint of the rolling ball bearing under the dynamic theoretical framework of a multi-body system was needed. Moreover, the model estab-

Fig. 1 A dynamic model of impact in a multi-body system with a rolling ball bearing joint



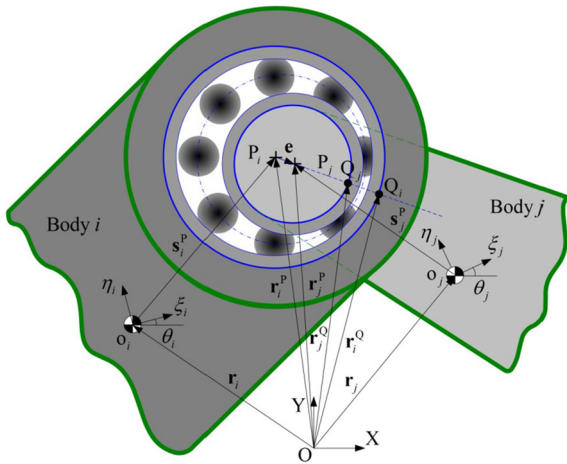


Fig. 2 Modelling of a rolling ball bearing joint in a planar multi-body system

lished should be capable of revealing the motion’s characteristics in the bearing and the characteristics of the contact force between rolling elements with the inner and outer raceways. Second, an effective impact force model of the contact of rigid bodies was needed.

2.1 Modelling a ball bearing joint in a planar multi-body system

Generally speaking, due to their being affected by the radial clearance of the rolling bearing, the inner and outer races of the bearing joint are prone to shift from the origin centre during the motion. Taking account of the radical elastic compressive deformation of the bearing under load, this shift will be more obvious. To accurately describe the eccentricity of the rolling ball bearing joint, it is necessary to obtain a general theoretical method of building the revolute joint of a rolling ball bearing under a multi-body dynamics theoretical framework, as shown in Fig. 2. The location vector centres of inner and outer races P_i and P_j in the coordinate system can be expressed by:

$$\mathbf{r}_z^P = \mathbf{r}_z + \mathbf{A}_z \mathbf{s}_z^P, \quad (z = i, j) \tag{2}$$

where, \mathbf{r}_z is the position vector of the body-fixed coordinate system origin of the two rigid bodies connected by bearing in generalised coordinate system XOY; \mathbf{s}_z^P is the position vector of the centres P_i and P_j of the inner and outer races in the body-fixed coordinate system; and \mathbf{A}_z is a transformation matrix.

By taking the derivative of Eq. (2) with respect to time t , we obtain the velocity vectors of the centre P_i and P_j of the inner and outer races (respectively) in generalised coordinates.

$$\dot{\mathbf{r}}_z^P = \dot{\mathbf{r}}_z + \dot{\mathbf{A}}_z \mathbf{s}_z^P, \quad (z = i, j) \tag{3}$$

If the radial internal clearance and the elastic contact deformation of the bearing are included, the inner and outer races will shift from the centre. The eccentricity vector and relative velocity vector can be represented as Eqs. (4) and (5), respectively:

$$\mathbf{e} = \mathbf{r}_j^P - \mathbf{r}_i^P \tag{4}$$

$$\mathbf{v} = \dot{\mathbf{r}}_j^P - \dot{\mathbf{r}}_i^P \tag{5}$$

The amplitude of the eccentricity vector is expressed as:

$$e = \sqrt{\mathbf{e}^T \mathbf{e}} \tag{6}$$

The unit normal vector to the direction of the eccentricity can be expressed as:

$$\mathbf{n}_e = \mathbf{e}/e \tag{7}$$

As shown in Fig. 2, the contact point of the outer race of bearing with the bush of the rigid body i is denoted as Q_i , while the contact point of the inner race of the bearing with the journal of a rigid body j is recorded as Q_j . The position vector of contact point Q_i and Q_j can be represented as:

$$\mathbf{r}_z^Q = \mathbf{r}_z + \mathbf{A}_z \mathbf{s}_z^P + R_z \mathbf{n}_e, \quad (z = i, j) \tag{8}$$

where, R_z ($z = i, j$) refers to the radius of bush and journal separately. According to this analysis, the relative eccentricity vector and eccentricity velocity vector of the races of the bearing can be obtained.

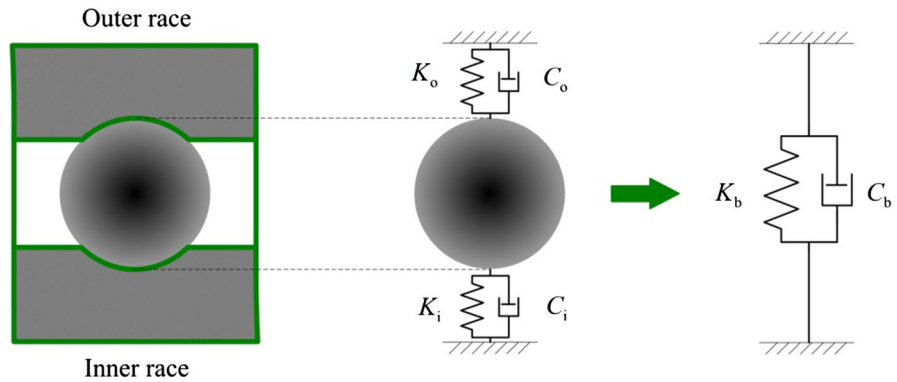
The contact force between a rolling ball and the rolling path in the inner and outer races of the bearing are given by:

$$F_r = K_b \delta_r^n + C_b v_r \tag{9}$$

where, K_b and C_b are the total stiffness and total damping of the rolling ball with the inner and outer raceways of the bearing, respectively; δ_r and v_r are separately the radical shift and relative eccentricity velocity in the direction of location angle ϕ_r ; n is a load-deformation index (for the ball bearing, it is 3/2 and for a roller bearing, it is equal to 10/9 [55]). As shown in Fig. 3, the stiffness of the contact between the rolling ball with the inner and outer raceways of bearing can be signified by:

$$K_{i,o} = \frac{2\sqrt{2} \left(\frac{E_b}{1-\nu_b^2} \right)}{3 \left(\sum \rho_{i,o} \right)^{1/2}} \left(\frac{1}{\delta_{i,o}^*} \right)^{3/2} \quad (\text{N/m}^{3/2}) \tag{10}$$

Fig. 3 Stiffness calculation in ball raceway contact



where, E_b and ν_b are the elastic modulus and Poisson’s ratio of the ball bearing elements, respectively. $\delta_{1,o}^*$ is the dimensionless deflection factor and $\sum \rho_{i,o}$ is the sum of the curvatures at the contact point.

The total stiffness K_b for a single ball element in contact with the inner and outer raceways is:

$$K_b = \left(\frac{1}{(1/K_i)^{2/3} + (1/K_o)^{2/3}} \right)^{3/2} \quad (\text{N/m}^{3/2}) \tag{11}$$

Generally, estimation of the damping of a ball bearing is difficult because of the dominant extraneous damping which swamps the damping of the bearing [56]. Based on experimental and theoretical studies, Dietl et al. [57] pointed out that the major contributions to bearing damping include: lubricant film damping in the rolling contacts, material damping due to Hertzian deformation of the rolling bodies, and damping at the interface between the outer ring and the bearing housing. Mitsuya et al. [58] experimentally investigated the damping of a 6,200-type deep-groove ball bearing. The experimental damping coefficients ranged between 150 and 350 Ns/m. Based on these experimental results, an appropriate damping value can be selected to ensure convergence of the numerical calculation.

It can be seen from Fig. 4 that, the radical shift of the rolling ball of the bearing in the direction of position angle ϕ_r can be calculated using Eq. (12):

$$\delta_r = e_x \cos \phi_r + e_y \sin \phi_r - \frac{1}{2} P_d \tag{12}$$

where, e_x and e_y are separately the components of eccentricity \mathbf{e} in directions X and Y; P_d refers to the radial clearance of the bearing.

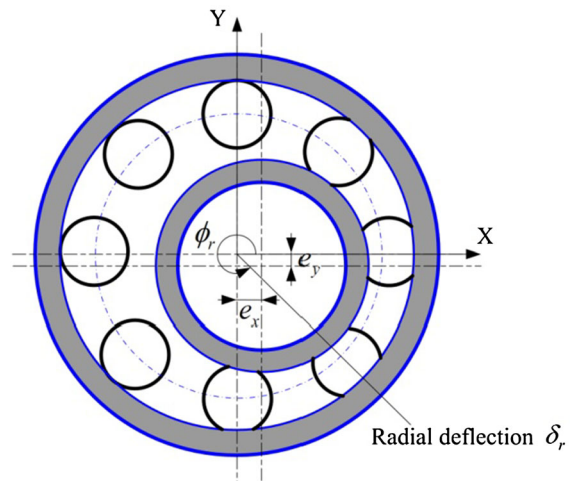


Fig. 4 Radial deflection at a general rolling ball position

In the direction of position angle ϕ_r , the relative eccentricity velocity is recorded as:

$$v_r = v_x \cos \phi_r + v_y \sin \phi_r \tag{13}$$

where, v_x and v_y are the components of relative velocity vector \mathbf{v} in directions X and Y.

In the assumption that the rolling balls are uniformly distributed in the rolling paths of inner and outer races at the same rotational speed, the angle position ϕ_r of the r th rolling ball at arbitrary time point t can be calculated by Eq. (14).

$$\phi_r = \frac{2\pi}{N_b} (r - 1) + \omega_m t, \quad (r = 1, 2, \dots, N_b) \tag{14}$$

where, N_b denotes the number of rolling balls in the bearing; ω_m is the angular velocity of a rolling ball (see Eq. (15)).

$$\omega_m = \frac{\omega_i d_i + \omega_o d_o}{d_i + d_o} \tag{15}$$

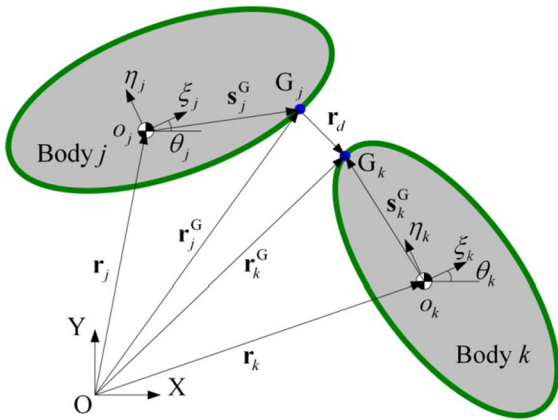


Fig. 5 Modelling of a contact constraint between two rigid bodies in a planar multi-body system

By substituting Eqs. (11), (12), and (13) into Eq. (9) and taking account of the influences of damping, we can obtain the contact force between the rolling ball and the rolling paths in the inner and outer races of the bearing.

2.2 Modelling of a contact constraint in a planar multi-body system

Figure 5 shows the contact constraint between rigid bodies j and k established in generalised coordinate system XOY . The position vectors of impact contact points G_j and G_k in the generalised coordinate system can be expressed as:

$$\mathbf{r}_u^G = \mathbf{r}_u + \mathbf{A}_u \mathbf{s}_u^G, \quad (u = j, k) \tag{16}$$

where, \mathbf{r}_u is the position vector of the body-fixed coordinate origin of the two rigid bodies connected by impact constraint under the generalised coordinate system; \mathbf{s}_u^G is the position vector of the contact points G_j and G_k of collision in the body-fixed coordinate system; and \mathbf{A}_z is a transformation matrix.

By taking the derivative of Eq. (16) with respect to time t , the velocity vector of the contact points G_j and G_k of the collision in generalised coordinates may be obtained.

$$\dot{\mathbf{r}}_u^G = \dot{\mathbf{r}}_u + \dot{\mathbf{A}}_u \mathbf{s}_u^G, \quad (u = j, k) \tag{17}$$

In the contact between the rigid bodies, the relative position vector and corresponding amplitude can be expressed by Eqs. (18) and (19), respectively.

$$\mathbf{r}_d = \mathbf{r}_k^G - \mathbf{r}_j^G \tag{18}$$

$$r_d = \sqrt{\mathbf{r}_d^T \mathbf{r}_d} \tag{19}$$

The unit normal vector to the direction of contact is calculated by:

$$\mathbf{n}_r = \mathbf{r}_d / r_d \tag{20}$$

Equations (21) and (22) represent the velocity components of the relative impact velocity between contact points G_j and G_k in the normal vector direction and tangential direction of the normal vector, respectively:

$$v_N = (\dot{\mathbf{r}}_k^G - \dot{\mathbf{r}}_j^G)^T \mathbf{n}_r \tag{21}$$

$$v_T = (\dot{\mathbf{r}}_k^G - \dot{\mathbf{r}}_j^G)^T \mathbf{t} \tag{22}$$

where, \mathbf{t} is obtained by rotating the normal vector \mathbf{n}_r in a counter-clockwise direction by 90° . After the relative penetration and velocities at the contact point have been determined, the normal contact and friction forces can be computed based on some contact force models and friction models.

An appropriate contact force model is crucial for the precise description of the collision dynamics between bodies. So far, a variety of contact force models have been proposed by: Hertz [59], Zukas et al. [60], Lankarani and Nikravesh [61], Dubowsky and Freudenstein [62], Johnson [63], Radzimovsky [64], Goldsmith [65] and Flores et al. [5]. It is worth noting that only the model developed by Lankarani and Nikravesh [61] is widely used in dynamic studies of mechanical multi-body systems with clearance joints. This is attributable to the simplicity of its contact force model, resulting ease of calculation, applicability to impact in multi-body systems, and rapid convergence due to the inclusion of energy dissipation modelling upon impact. In an academic monograph, Flores et al. [66] compared different contact force models and proved the effectiveness of the model proposed by Lankarani and Nikravesh when describing the dynamic properties in the contact impact of a clearance joint. Besides, he confirmed that Lankarani and Nikravesh’s model can be transformed to deal with contact problems between cylindrical surfaces. Therefore, the continuous contact force model of Lankarani and Nikravesh was used to depict the contact impact between clearance joints in the present study.

Using Lankarani and Nikravesh’s continuous contact force model [58], the impact force when rigid

body j and k come into contact at point G can be denoted by:

$$\tilde{F} = K_d \delta_d^{1.5} \left(1 + \frac{3(1 - e_c^2)}{4} \frac{\dot{\delta}_d}{\delta_d^{(-)}} \right) \quad (23)$$

where, $\dot{\delta}_d$ is the relative impact velocity; $\delta_d^{(-)}$ is the initial impact velocity; e_c is a coefficient of restitution; and K_d is the contact stiffness. The contact stiffness K_d can be calculated by Eqs. (24) and (25):

$$K_d = \frac{4}{3\pi (h_j + h_k)} \left(\frac{\tilde{R}_j \tilde{R}_k}{\tilde{R}_j + \tilde{R}_k} \right)^{1/2} \quad (24)$$

$$h_u = \frac{1 - \tilde{\nu}_u^2}{\pi \tilde{E}_u}, \quad (u = j, k) \quad (25)$$

where, $\tilde{\nu}_u$ is the Poisson’s ratio of the rigid bodies in collision; \tilde{E}_u is the modulus of elasticity of the rigid bodies in the collision; \tilde{R}_u is the curvature radius of the contact point for the collision. As shown in Eq. (23), it is crucial to obtain the coefficient of restitution accurately to calculate the contact force and the dynamic response of the system. However, in reality, the coefficient of restitution needs to be measured in experiments rather than being calculated/deduced [67]. Further explanation lies beyond the scope of this study.

In addition to the normal reaction forces, a friction force can be included to enhance the model. Dubowsky [68], Rooney and Deravi [69], Threlfall [70], Karnopp [71], and Ambrósio [72] have established different friction models. In research concerning the dynamics of multi-body systems with joint clearance, Ambrósio’s friction force model is widely applied. The mathematical expression of this frictional force model is:

$$F_T = -\mu c_d F_N \frac{\mathbf{v}_T}{|\mathbf{v}_T|} \quad (26)$$

where c_d is a dynamic correction coefficient expressed by:

$$c_d = \begin{cases} 0 & \text{if } v_T \leq v_0 \\ \frac{v_T - v_0}{v_1 - v_0} & \text{if } v_0 \leq v_T \leq v_1 \\ 1 & \text{if } v_T \geq v_1 \end{cases} \quad (27)$$

in which, v_0 and v_1 are the given tolerances for the velocity. Compared with the other three friction models, the great merit of this friction force model is that the correction factor can prevent the friction force from changing direction when the value of the tangential velocity approaches zero: this allows numerical stabilisation of the integration algorithm.

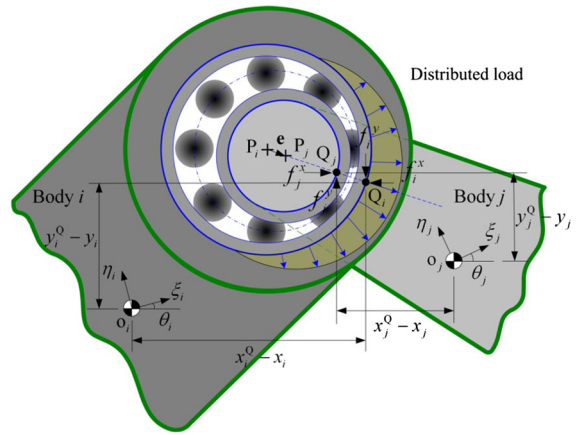


Fig. 6 The contact load distribution in the bearing joint

2.3 The generalised force on the impacted planar multi-body system with a ball bearing joint

2.3.1 The generalised force in the bearing joint

The joint rolling element bearing will be affected by inertial load in the movement of the mechanical multi-body system. Figure 6 describes the load distribution of the rolling ball bearing joint under the influences of inertial load. Due to the existence of radial clearance in the bearing, some rolling balls are affected while some are unaffected by the load at time t . As shown in Fig. 6, even in the loaded region, the loads on different rolling balls are different. In addition, since the amplitude and direction of the inertial load on the bearing varies with the movement of the mechanical multi-body system, the loads on the rolling balls of the bearing face are governed by a complex variational relationship. Obviously, the distribution law for the loads in the bearing is affected by the radial clearance, eccentricity vector variations, and the motional characteristics of the bearing. If the influences of elastic compressive deformation are included, the loads on the rolling balls are given by Eq. (9).

In the generalised coordinate system, the equivalent constraint force of the bearing joint can be deduced using the elastic contact force on each rolling ball as given by:

$$\begin{bmatrix} F_x \\ F_y \end{bmatrix} = \sum_{r=1}^{N_b} F_r \begin{bmatrix} \cos \phi_r \\ \sin \phi_r \end{bmatrix} \quad (28)$$

As shown in Fig. 6, the joint forces of rigid body i and its corresponding torque on the centroid of the rigid body are:

$$\mathbf{f}_i = \begin{bmatrix} F_x \\ F_y \end{bmatrix}, T_i^f = -(y_i^Q - y_i) f_i^x + (x_i^Q - x_i) f_i^y \quad (29)$$

In similar way, the forces on the joint of rigid body j and its corresponding torque on the centroid of the rigid body are:

$$\mathbf{f}_j = - \begin{bmatrix} F_x \\ F_y \end{bmatrix}, T_j^f = (x_j^Q - x_j) f_j^y - (y_j^Q - y_j) f_j^x \quad (30)$$

where, $x_i^Q - x_i$ and $y_i^Q - y_i$ separately represent the distances from contact point Q_i to the centroid of rigid body i in the X and Y directions; $x_j^Q - x_j$ and $y_j^Q - y_j$ separately refer to the distances from contact point Q_i to the centroid of rigid body j in the X and Y directions.

In the hypotheses above, we neglected rolling friction between the rolling balls and the rolling paths in the bearing. Therefore, friction was not taken into consideration in establishing the generalised external force on the rolling ball bearing joint. The reason for this simplification is that the rolling element bearing has a structural feature of multi-point contacts between rolling elements and raceways. A detailed description of the friction effect in each contact is complex and the simulation would be time-consuming. To simplify the computational model, only the normal contact forces in bearing multi-point contacts were considered by the authors. On the other hand, the rolling friction in ball and raceway contact is usually quite small and has a smaller effect on the dynamic response of such bearing systems: many researchers [42–45, 47–49] examining rolling element bearing dynamics neglect frictional effects.

2.3.2 The generalised force caused by external impact

The impact, in which rigid body j collides with rigid body k , gives rise to the normal contact force and tangential frictional force at the contact point of the collision. Normal contact forces are calculable using Eq. (23), while tangential frictional force is found using a frictional force model, such as the Ambrósio [72] friction model. As shown in Fig. 7, the direction of the normal passing through the contact point and vertical to the contact plane is defined as the direction of the contact force.

As suggested by Fig. 8, the contributions to the generalised vector of forces and moments working on bodies j and k can be found by projecting the normal force onto the normal direction \mathbf{n}_r , that is:

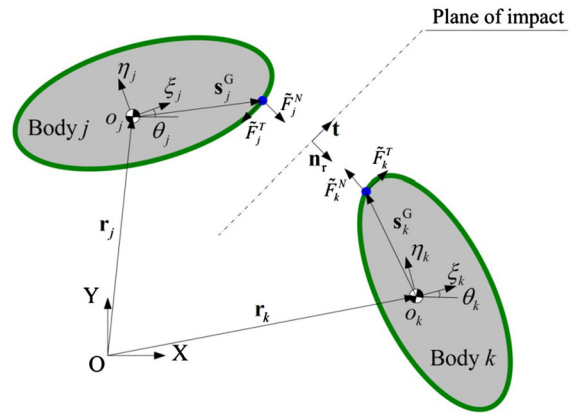


Fig. 7 The force vectors for two rigid bodies in contact

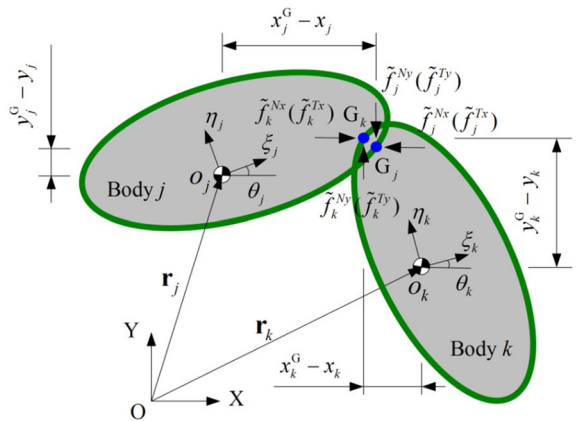


Fig. 8 The contributions to the generalised force vectors and moments on contact bodies

$$\begin{aligned} \tilde{\mathbf{f}}_j^N &= \tilde{F}_j^N \mathbf{n}_r = \begin{bmatrix} \tilde{f}_j^{Nx} \\ \tilde{f}_j^{Ny} \end{bmatrix}, \\ \tilde{\mathbf{f}}_k^N &= \tilde{F}_k^N \mathbf{n}_r = \begin{bmatrix} \tilde{f}_k^{Nx} \\ \tilde{f}_k^{Ny} \end{bmatrix}, \tilde{F}_k^N = -\tilde{F}_j^N \end{aligned} \quad (31)$$

$$\begin{aligned} \tilde{T}_j^N &= (y_j^G - y_j) \tilde{f}_j^{Nx} - (x_j^G - x_j) \tilde{f}_j^{Ny}, \\ T_k^N &= -(x_k^G - x_k) \tilde{f}_k^{Ny} - (y_k^G - y_k) \tilde{f}_k^{Nx} \end{aligned} \quad (32)$$

Similarly, contributions from the tangential force can be found by projecting the tangent force onto the plane of collision, *i.e.* the direction \mathbf{t} , perpendicular to the normal direction \mathbf{n}_r :

$$\begin{aligned} \tilde{\mathbf{f}}_j^T &= \tilde{F}_j^T \mathbf{t} = \begin{bmatrix} \tilde{f}_j^{Tx} \\ \tilde{f}_j^{Ty} \end{bmatrix}, \tilde{\mathbf{f}}_k^T = \tilde{F}_k^T \mathbf{t} = \begin{bmatrix} \tilde{f}_k^{Tx} \\ \tilde{f}_k^{Ty} \end{bmatrix}, \\ \tilde{F}_k^T &= -\tilde{F}_j^T \end{aligned} \quad (33)$$

$$\begin{aligned} \tilde{T}_j^T &= (y_j^G - y_j) \tilde{f}_j^{Tx} - (x_j^G - x_j) \tilde{f}_j^{Ty}, \\ T_k^T &= -(x_k^G - x_k) \tilde{f}_k^{Ty} - (y_k^G - y_k) \tilde{f}_k^{Tx} \end{aligned} \quad (34)$$

where, $x_j^G - x_j$ and $y_i^G - y_i$ separately represent the distances from contact point G_j to the centroid of rigid body j in the X and Y directions; $x_k^G - x_k$ and $y_k^G - y_k$ separately refers to the distances from contact point G_k to the centroid of rigid body k in the X and Y directions.

2.4 The equations of motion of an impacted planar multi-body system with a bearing joint

Based on the analysis above, the joint forces of rigid bodies i and j and corresponding torques on the centroids of the rigid bodies may be obtained using Eqs. (29) and (30), respectively. Moreover, using Eqs. (31)–(34), the normal contact forces and tangential frictional forces on rigid bodies j and k , as well as the torques they generate on the centroids of the rigid bodies can be obtained. If these forces and torques are taken as generalised forces and substituted into the dynamic equations for the multi-body system, the equation of motion

of the impacted multi-body system with a rolling ball bearing joint can be obtained, as shown below:

$$\begin{bmatrix} \mathbf{M} & \Phi_q^T \\ \Phi_q & \mathbf{0} \end{bmatrix} \begin{bmatrix} \ddot{\mathbf{q}} \\ \lambda \end{bmatrix} = \begin{bmatrix} \mathbf{Q}^A \\ \gamma \end{bmatrix} \quad (35)$$

where, \mathbf{M} is the mass matrix of the system; Φ_q is the Jacobian matrix of constraint equations; $\ddot{\mathbf{q}}$ is an acceleration vector; \mathbf{Q}^A is the generalised external force vector; λ is a Lagrange multiplier; and vector $\gamma = -(\Phi_q \dot{\mathbf{q}})_q \dot{\mathbf{q}} - 2\Phi_{qt} \dot{\mathbf{q}} - \Phi_{tt}$.

Unfortunately, the equation above is prone to error. Moreover, with the prolongation of the simulation, the error grows and results in inaccuracy. To guaranteeing the stability of the numerical solution and to ensure correct results, the Baumgarte stabilisation method [73] was used here. The values of the parameters $\alpha = \beta = 5$ are used [74] in control equation $\ddot{\Phi} + 2\alpha\dot{\Phi} + \beta^2\Phi = 0$ in the simulations.

$$\begin{bmatrix} \mathbf{M} & \Phi_q^T \\ \Phi_q & \varphi \end{bmatrix} \begin{bmatrix} \ddot{\mathbf{q}} \\ \lambda \end{bmatrix} = \begin{bmatrix} \mathbf{Q}^A \\ \gamma - 2\alpha\dot{\Phi} - \beta^2\Phi \end{bmatrix} \quad (36)$$

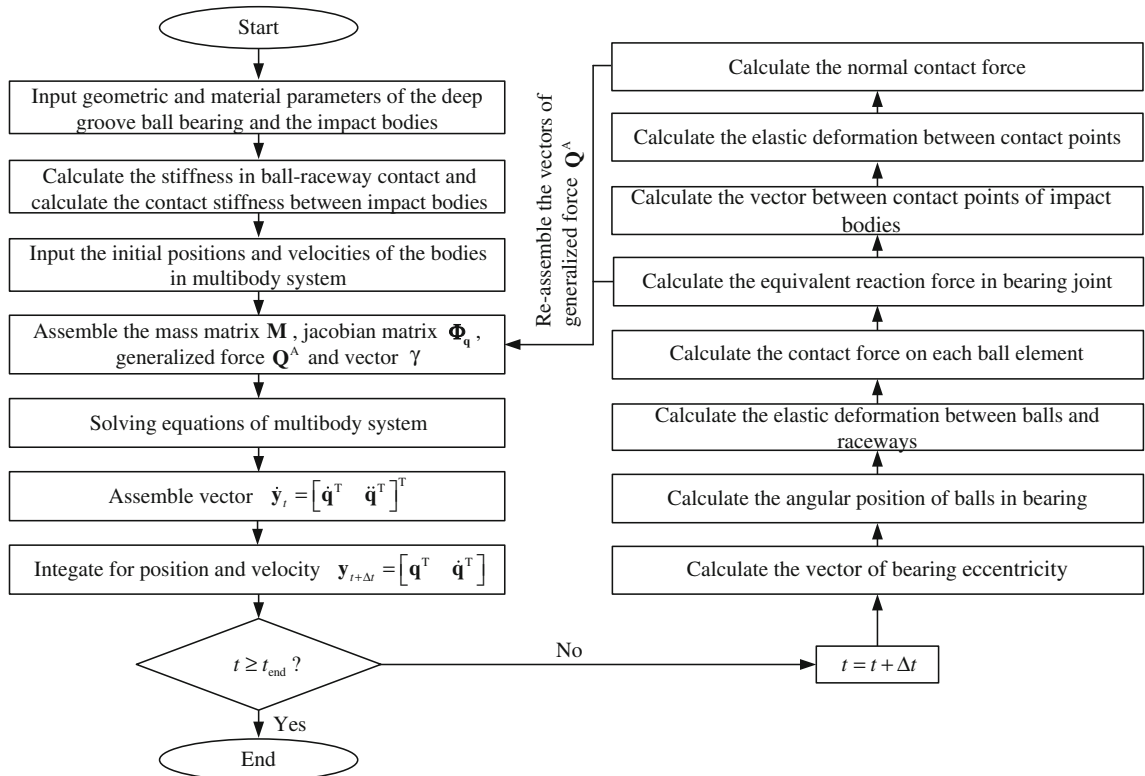


Fig. 9 Flowchart of the computational procedure for the dynamic analysis of the impacted multi-body system with deep groove ball bearing joints

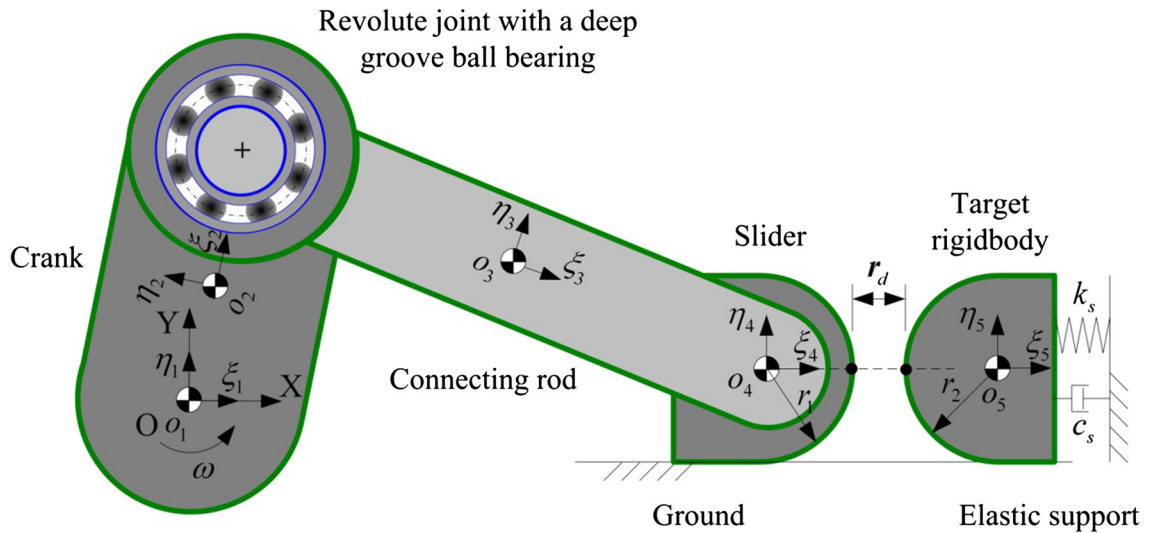


Fig. 10 An impact slider–crank mechanism with a deep groove ball bearing joint

Furthermore, Fig. 9 shows the flowchart for the computational procedure for dynamic analysis of the impacted multi-body system with its ball bearing joint.

3 Numerical simulation

3.1 An impact slider–crank mechanism with a ball bearing joint

In this section, we analysed an impacted multi-body system composed of a slider–crank mechanism containing a deep groove ball bearing and the target rigid body with its elastic support. Figure 10 shows the dynamic model of this system: the crank and connecting rod are connected by a deep groove ball bearing (SKF 98205). The bearing in this position not only rotates, but also undergoes translational motion along with the slider–crank mechanism. The reason why this joint was selected was because its inertial load variation was more complex than the other two revolute joints in the motion of the mechanism. The variation of the contact force on each rolling ball element over an entire rotation cycle of this bearing is readily obtained and analysed. The outer and inner races of the rolling bearing are fixedly connected with the bush on the crank and the journal of the connecting rod, respectively. The slider and target rigid body are restricted in the collision. With the movement of the slider–crank mechanism, the slider and target rigid body will collide with

each other when they satisfy the position constraints for contact. In addition, the target rigid body is elastically supported on the ground. When affected by the impact force, the compressive spring of the target rigid body moves to the right. When the slider is separated from the target rigid body, such elastic compressive deformation recovers gradually.

Table 1 lists the geometric and inertial parameters of the slider–crank mechanism with the target rigid body in collision. Table 2 lists the geometric structural parameters and material attributes of the deep groove ball bearing (SKF 98205). Figure 11 shows the geometrical characteristics of the deep groove ball bearing. Taking the specific geometric parameters of the bearing and substituting the appropriate values into the related formulae, the contact stiffness between the rolling balls and both the inner and outer races of the bearing was 2.57 and 2.86×10^{10} N/m separately. Then, the total contact stiffness was calculated to have been 9.57×10^9 N/m. A damping value of 300 Ns/m was applied to the contact vibration arising between each rolling ball and the raceways ensure convergence of the numerical analysis and its calculations. Table 3 lists some necessary parameters for the solution of the numerical example. Table 4 lists the initial parameters of the slider–crank mechanism and target rigid body, including initial position and initial speed. At the beginning, it is assumed that crank and connecting rod lie in the same horizontal line. Moreover, to guarantee a smooth simulation calculation, we assumed that the impact con-

Table 1 Dimensions and mass parameters for the impact slider–crank mechanism

Bodies	Length (mm)	Mass (kg)	Moment of inertia (kg mm ²)
Crank	50	0.75	520
Connecting rod	120	0.67	1, 200
Slider	—	0.3	—
Target rigid body	—	0.1	—

Table 2 Geometric and material properties for the deep groove ball bearing (SKF 98205)

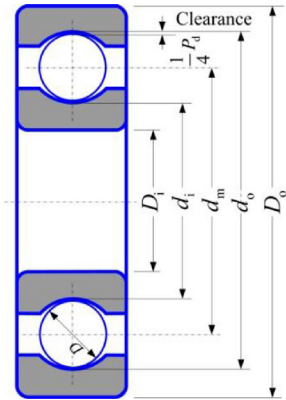


Fig. 11 Geometrical characteristics of the deep groove ball bearing.

Parameters	Values
Bore diameter, D_i	25 mm
Outer diameter, D_o	52 mm
Pitch diameter, d_m	37.9 mm
Inner raceway diameter, d_i	29.2 mm
Outer raceway diameter, d_o	46.6 mm
Ball diameter, D	8.7 mm
Radial clearance, P_d	0.04 mm
Number of balls, N_b	8
Young's modulus of bearing material, E_b	207 GPa
Poisson's ratio of bearing material, ν_b	0.3

Table 3 Parameters used in the impact dynamic simulations

Parameters	Values
Crank speed, ω	600 rpm
Coefficient of restitution, e_c	0.9
Coefficient of friction, μ	0
Young's modulus of contact bodies, \tilde{E}	207 GPa
Poisson's ratio of contact bodies, $\tilde{\nu}$	0.3
Supporting stiffness, k_s	100 kN/m
Supporting damping, c_s	120 Ns/m
Contact radius of slider, r_1	0.01 m
Contact radius of target rigid body, r_2	0.01 m
Integration step size	0.00001 s
Integrator scheme	Gear
Baumgarte stability control parameters α, β	5, 5

straint between slider and target rigid body functioned after the crank turned through 180°. In addition, since the contact between the slider and the target rigid body is considered to be a contact between circular arc surfaces, and slider and target rigid body merely moves horizontally: the influences of friction in the contact are ignored.

3.2 Results and discussion

Figure 12 shows the dynamic responses of slider and target rigid body over a complete motion period of the slider–crank mechanism, involving the displacements, velocities, and accelerations of the slider and target rigid body. As shown in the displacement response in Fig. 12a, if the real distance between the slider and target rigid body failed to satisfy the impact constraints, collision did not occur and target rigid body remained stable. With the continuous motion of the mechanism, impact will be induced when the real distance between slider and target rigid body meet the contact constraints on position. Meanwhile, under the impact of the slider, the target body generates displacement variation by compressing the support spring. As time goes on, the rigid body separates from the slider and recovers to its initial position with the help of the supporting spring. In addition, the responses of velocity and acceleration (Fig. 12b, c) imply that the impact between the slider and the rigid body shows a large vibration amplitude when collision occurs instantaneously. Subsequently, the vibration amplitude of the impact decays gradually and the sliding block and target rigid body move

Table 4 The initial values of the impact slider–crank mechanism necessary to start the dynamic analysis

Crank speed (rpm)	The initial positions											
	Crank			Connecting rod			Slider			Target rigid body		
	ξ_2 (mm)	η_2 (mm)	θ_2 (rad)	ξ_3 (mm)	η_3 (mm)	θ_3 (rad)	ξ_4 (mm)	η_4 (mm)	θ_4 (rad)	ξ_5 (mm)	η_5 (mm)	θ_5 (rad)
600	25	0	0	110	0	0	170	0	0	180	0	0
Crank speed (rpm)	The initial velocities											
	Crank			Connecting rod			Slider			Target rigid body		
	$\dot{\xi}_2$ (mm/s)	$\dot{\eta}_2$ (mm/s)	$\dot{\theta}_2$ (rad/s)	$\dot{\xi}_3$ (mm/s)	$\dot{\eta}_3$ (mm/s)	$\dot{\theta}_3$ (rad/s)	$\dot{\xi}_4$ (mm/s)	$\dot{\eta}_4$ (mm/s)	$\dot{\theta}_4$ (rad/s)	$\dot{\xi}_5$ (mm/s)	$\dot{\eta}_5$ (mm/s)	$\dot{\theta}_5$ (rad/s)
600	0	1,570.8	62.83	0	1,570.8	−26.18	0	0	0	0	0	0

in close contact until separation. When the slider was completely separated from the target rigid body, the free vibration gradually attenuates under the spring damping effect.

Figure 13 shows the variation characteristics of the contact force between the slider and the target rigid body. It is observed that at the instant of the collision, the contact impact force between slider and target rigid body varied significantly. In this process, there are two situations arising between the slider and the target rigid body, namely, contact and separation. In detail, the contact of the slider and target rigid body gives rise to an instant collision force of high amplitude, while the impact forces instantly decrease to zero upon separation. In the initial stage of the impact between the slider and target rigid body, the contact and separation are repeated several times. Moreover, due to the energy loss in the collision, the impact force gradually decays before the following contact. In the late stage of the collision, the contact force is smooth owing to the close contact between the slider and target rigid body. Until the separation of the slider from the target rigid body, the contact force between the two decreases to zero.

Figure 14 shows the variations of equivalent reaction force of the rolling ball bearing joint in the slider–crank mechanism. It is observed that the impact between the slider and the target rigid body causes violent variations in the dynamic loading of rolling ball bearing joint. At the instant of collision, the equivalent reaction force on the bearing joint shows sudden changes in amplitude. In the impact, it fluctuates with repeated occurrences of the contact and separation of the slider and target rigid body with a gradually reducing amplitude attributable to the gradual loss of the energy in the collision. It

should be noted that the equivalent reaction force of the bearing joint shows small amplitude fluctuations when the slider had completely separated from the target rigid body. These fluctuations are mainly induced by the inertial load variations in the bearing joint after the slider separated from the target rigid body.

Generally, the distribution characteristics of the load on the rolling ball bearing joint are mainly affected by the radial clearance of the bearing, the inertial load on the joint, and the kinetic properties of the bearing. Since the inertial load on the bearing and the positions of the rolling balls are in constant variation with the movement of the mechanism, the variation of the load on the rolling balls of the bearing joint differed from ball to ball. That is to say, at certain positions of the mechanism, some rolling balls are stressed while others in the bearing are free from load. Even if the rolling balls were simultaneously located in the loaded region, the amplitude of the load thereon differed from ball to ball.

Figure 15 shows the variations of the contact loads on the rolling balls in the bearing joint when the slider–crank mechanism was at collision and free from collision, respectively. It can be found that, in the free-from-collision condition, the balls 1 and 8 in the bearing were free from load over an entire period of slider–crank mechanism motion (from 0.04 to 0.14 s). Meanwhile, balls 2–7 are loaded differently.

Table 5 lists the load amplitude on each rolling ball in the bearing throughout a complete motional period of the slider–crank mechanism. As shown, given certain positions, or times, in the slider–crank mechanism's cycle, the load on the rolling balls of the bearing presents different amplitudes and variation properties.

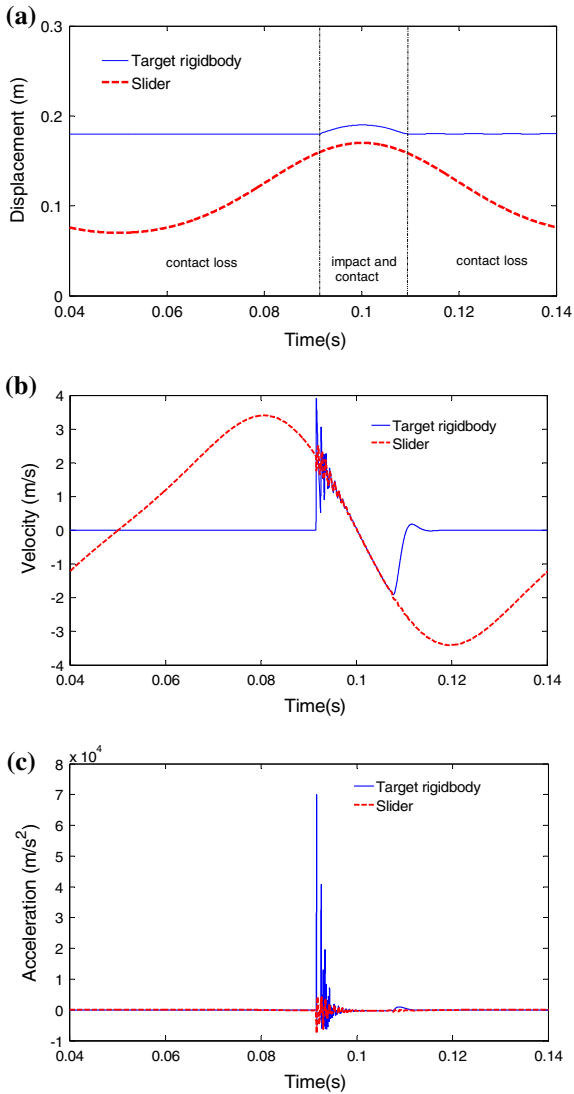


Fig. 12 Dynamic responses of the slider and target rigid body: **a** displacement, **b** velocity, **c** acceleration

It should be noted that, Fig. 15 merely illustrates the variation of the loads on the rolling balls of the bearing in one motional period of the slider–crank mechanism. Considering that the angular position directions of the rolling balls in the bearing vary with the movement of the slider–crank mechanism, that is to say, the rolling balls in the bearing were distributed at different angular positions under different motional periods of the slider–crank mechanism, the variations in loads on the rolling balls differed during each cycle.

Additionally, as shown in Fig. 15, if the impact effect of the slider–crank mechanism is excluded, the contact

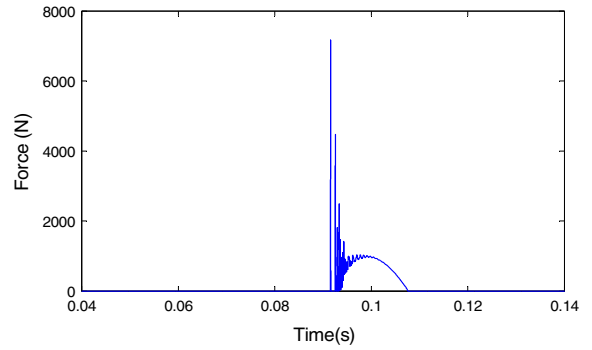


Fig. 13 Variation of the contact impact force between slider and target rigid body

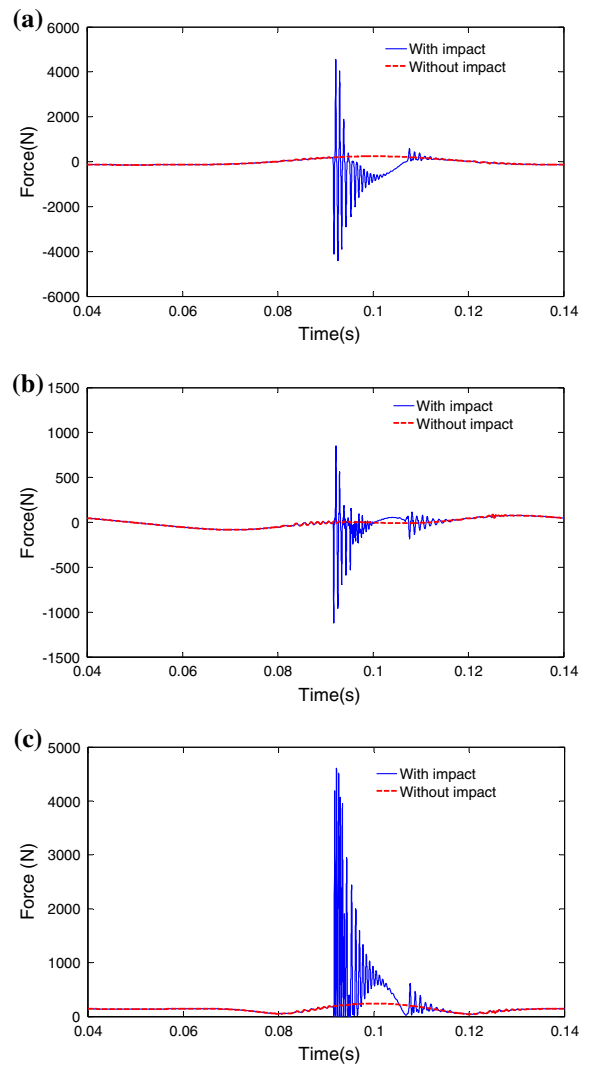


Fig. 14 Variations of the equivalent reaction force: **a** force in *x*-direction, **b** force in *y*-direction **c** force amplitude

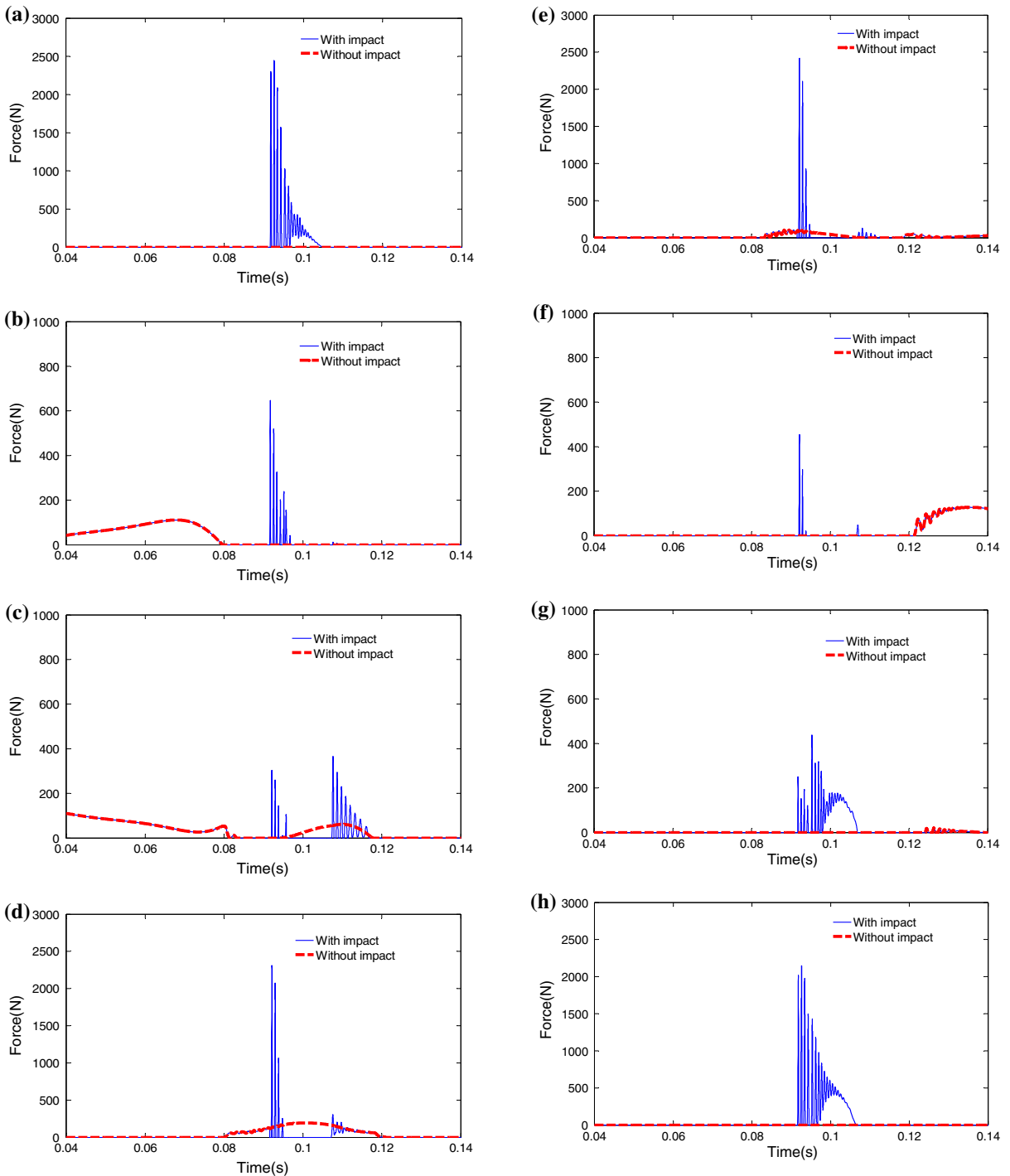


Fig. 15 Variation of the contact force on each rolling ball: **a** Ball 1, **b** Ball 2, **c** Ball 3, **d** Ball 4, **e** Ball 5, **f** Ball 6, **g** Ball 7, **h** Ball 8

loads on the rolling balls of the bearing fluctuate more smoothly. However, in case of including the collision effect arising from the target rigid body, the contact

Fig. 15 continued

loads on the rolling bodies in the bearing were subjected to sudden changes due to this external impact. Besides, since the rolling balls were located at different angular position directions, the external impact force of the

system exhibits different influences on the variations of contact load on the rolling balls. Generally speaking, research concerning the fatigue lifetime and reliability of the bearing is based on the analysis of its load characteristics. The present study offers an effective way of exploring the distribution characteristics of dynamic loads on the bearing in the case where the mechanical multi-body system suffers external impact(s). Moreover, it provides support for the performance evaluation, dynamic design, and geometric parameter optimisation of joints involving rolling ball bearings.

4 Verification of the approach: a simulation of the impact slider–crank mechanism with a ball bearing joint as modelled by MSC.ADAMS software

In this section, we established a virtual prototype model of an impacted slider–crank mechanism using MSC.ADAMS software, as shown in Fig. 16. In this model, the crank is fixed to the ground using an ideal revolute joint; the connecting rod is also linked to the slider using an ideal revolute joint; the deep groove bearing between the crank and connecting rod was taken as a revolute joint for connection purposes. The impact function in the software was used to model the contact force in the ball bearing joint. The slider and target rigid body are connected with the ground using ideal translational joints. Impact constraints are established between the slider and the target rigid body. The contact stiffness was 1.07×10^{10} N/m as calculated by Eq. (24). In addition, in the virtual prototype model, the slider is simplified into a cylinder and the target rigid body connected to the ground using a support spring.

In the plane of motion of the virtual mechanism, the geometric and inertial parameters of the crank, connecting rod, slider, and target rigid body are in agreement with the parameters of the theoretical model established in this study. The advantages of the model lie in its ability to involve the real geometric structural characteristics of the deep groove ball bearing and the complex contact relationships of the internal components in the bearing. As shown in Fig. 17, the contact relationships between the rolling balls with the inner race, outer race, and cage are defined in the ADAMS software. Table 6 lists the mass and inertial parameters of the components in the bearing, as well as the contact stiffness, contact damping, and frictional coefficients between compo-

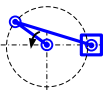
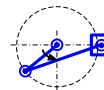
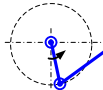
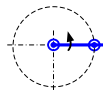
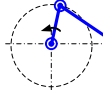
nents. Constricted by the constraint forces of the cage, the rolling balls were uniformly distributed around the rolling paths of the inner and outer races of the bearing.

In the simulation of the virtual prototype model, the bearing rotates with the motion of the slider–crank mechanism. Moreover, due to the interaction of the contact forces between the inner and outer races, rolling balls, and cage, the cage will rotate with the rolling balls. Figure 18 shows the variations of the displacement of the rotational angle of the cage in a complete motional period of the slider–crank mechanism. It can be found that, the rotational angle displacements of the cage in the bearing simulated by ADAMS are consistent with the results yielded by the theoretical method proposed in this study. Figure 19 shows the variations of the angular velocities of the cage in the bearing. It can be found that the angular velocity of the cage obtained in the ADAMS simulation exhibits larger variations due to the changes of the complex contact forces between the components of the bearing. However, since the motional variations of the cage are controlled by kinematic constraints in the theoretical model proposed in this study, *i.e.* in Eq. (14), the angular velocities of the rolling balls in the bearing show no variations in the theoretical analysis, heed should be paid to the fact that, upon impact between the slider and the target rigid body, the angular velocity of the cage in the bearing generates violent fluctuations due to the impact, as shown in Fig. 19. Upon separation of the slider from the target rigid body, it also showed larger variations.

Figure 20 shows the influences of the external impact on the load variations of the rolling balls of the bearing. Comparison of these results indicated that the theoretical method proposed in this study yielded a basically consistent variation law for the contact loads on the rolling balls of the bearing with both that and the ADAMS simulation results. The effectiveness of the theoretical method proposed in this study was thereby verified.

It is notable that the contact stiffness of the rolling balls with the inner and outer races of the bearing was 2.57 and 2.86×10^{10} N/m separately as calculated by Eq. (10). However, in the ADAMS virtual prototype model, they were 2.57 and 2.86×10^6 N/m, respectively. The reason for this discrepancy was that, if the contact stiffness of the rolling balls with the inner and outer races of the bearing in the virtual prototype model echoes the theoretical values, the ADAMS simulation tends to shift from the convergent results. This was

Table 5 Contact force statistics for each ball element in bearing joint at different positions of the slider–crank mechanism

Ball elements					
	$t = 0.04 \text{ s}$	$t = 0.06 \text{ s}$	$t = 0.08 \text{ s}$	$t = 0.1 \text{ s}$	$t = 0.12 \text{ s}$
Ball 1	0 N	0 N	0 N	0 N	0 N
Ball 2	42.9 N	92.2 N	0 N	0 N	0 N
Ball 3	109.7 N	64.8 N	53.1 N	24.9 N	0 N
Ball 4	0 N	0 N	0 N	193.8 N	0 N
Ball 5	0 N	0 N	0 N	45.1 N	40.7 N
Ball 6	0 N	0 N	0 N	0 N	0 N
Ball 7	0 N	0 N	0 N	0 N	0 N
Ball 8	0 N	0 N	0 N	0 N	0 N

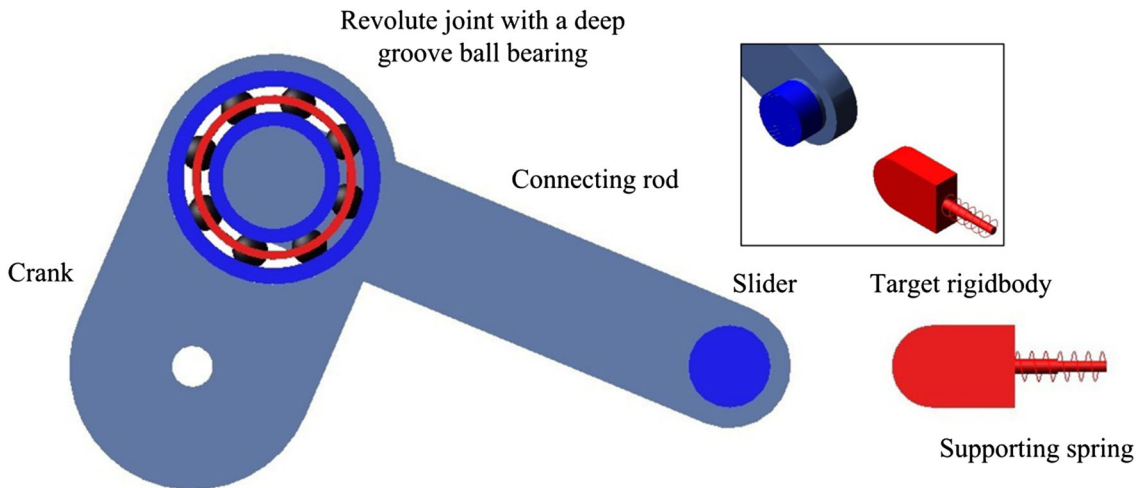


Fig. 16 An ADAMS model of the impact slider–crank mechanism with a rolling ball bearing joint

attributable to the idea that the contacts between the rolling balls with the inner and outer races of the bearing were a type of smooth curve surface contact. However, the ADAMS software is prone to develop errors in the accurate description of complex three-dimensional curved surface, as shown in Fig. 6. In the contact, tiny fluctuations in geometry would result in large contact forces. The stability of the simulation is thereby difficult to ensure. Moreover, there are complex multi-point contacts in the rolling ball bearing. The more numerous the contact points, the higher the contact stiffness, and the harder the ADAMS simulation. Therefore, to reduce the difficulty of ADAMS simulation and guarantee the convergence of the numerical calculation, the

contact stiffness of the rolling balls with the inner and outer races of the bearing should be much smaller than those used in theoretical calculations.

Additionally, Fig. 20 reveals that, in the collision between the slider and the target rigid body, the contact load of the bearing obtained by the theoretical method proposed in this study showed large fluctuation amplitude and high fluctuation frequency. This was because of the differences in the contact stiffness of the rolling balls with the inner and outer races of the bearing in the theoretical model and the ADAMS virtual model.

In the last part of this paper, the computational efficiency, when simulating the impact slider–crank mechanism with its rolling ball bearing joint, is discussed.

Table 6 The parameters of the deep groove ball bearing modelled by MSC.ADAMS software

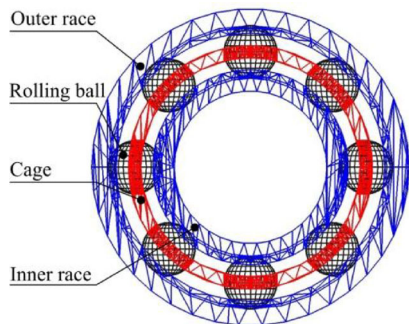


Fig. 17 The deep groove ball bearing in ADAMS software.

Parameters	Values
Contact stiffness, damping and friction between ball and outer raceway	2.86×10^6 N/m, 3×10^2 Ns/m, 0.01
Contact stiffness, damping and friction between ball and inner raceway	2.57×10^6 N/m, 3×10^2 Ns/m, 0.01
Contact stiffness, damping and friction between ball and cage	1×10^6 N/m, 1×10^3 Ns/m, 0
Mass and inertia of ball element	2.69×10^{-3} kg, 2.03×10^{-8} kg·m ²
Mass and inertia of outer race	4.08×10^{-2} kg, 2.411×10^{-5} kg·m ²
Mass and inertia of inner race	1.97×10^{-2} kg, 3.89×10^{-6} kg·m ²
Mass and inertia of cage	1.11×10^{-2} kg, 3.99×10^{-6} kg·m ²

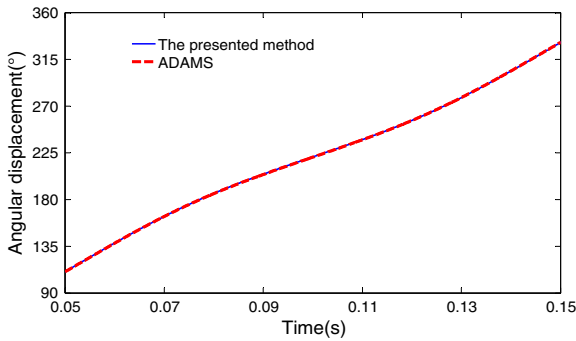


Fig. 18 Variation in the angular displacement of the bearing cage

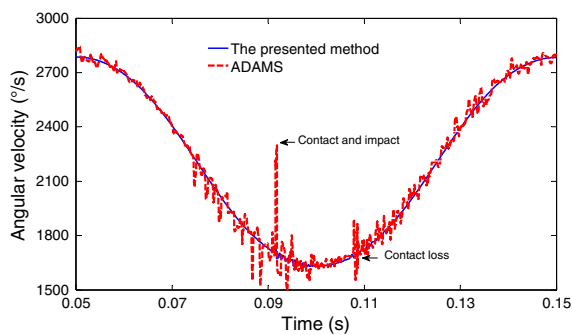


Fig. 19 Variation in the angular velocity of the bearing cage

For this, a DELL computer (CPU 3.1 GHz) was used to perform the calculations. Suppose that the total simulation time was 0.1 s (a whole period of the motion), then the computational time required for complete numeri-

cal simulations was 194 s. The ADAMS software took 685 s to finish the same work. Comparison with the ADAMS simulation model suggested that the theoretical method proposed in this study had a higher model solution efficiency.

5 Conclusions

This study proposed a modelling method to describe the dynamic behaviour of a mechanical multi-body system containing a rolling ball bearing joint under impact. With this method, the connection between rigid bodies and a bearing joint was established based on joint force constraints. Moreover, the impact constraints between a multi-body system and a target rigid body were developed using a continuous contact force model. Based on the theoretical method proposed, an impact multi-body system, which comprised a slider–crank mechanism containing a deep groove ball bearing and the target rigid body with its elastic support, was analysed to explore the dynamic response of such a complex discontinuous dynamic system and the variation of the dynamic load on the rolling ball bearing joint. In addition, multi-body dynamic simulation software (MSC.ADAMS) was used to build a virtual prototype of this impact slider–crank system. Analysis and comparison of the results proved the effectiveness of the theoretical method proposed in this study.

The results suggested that the external impact of the mechanical multi-body system was prone to inducing sudden changes of the equivalent reaction force on the

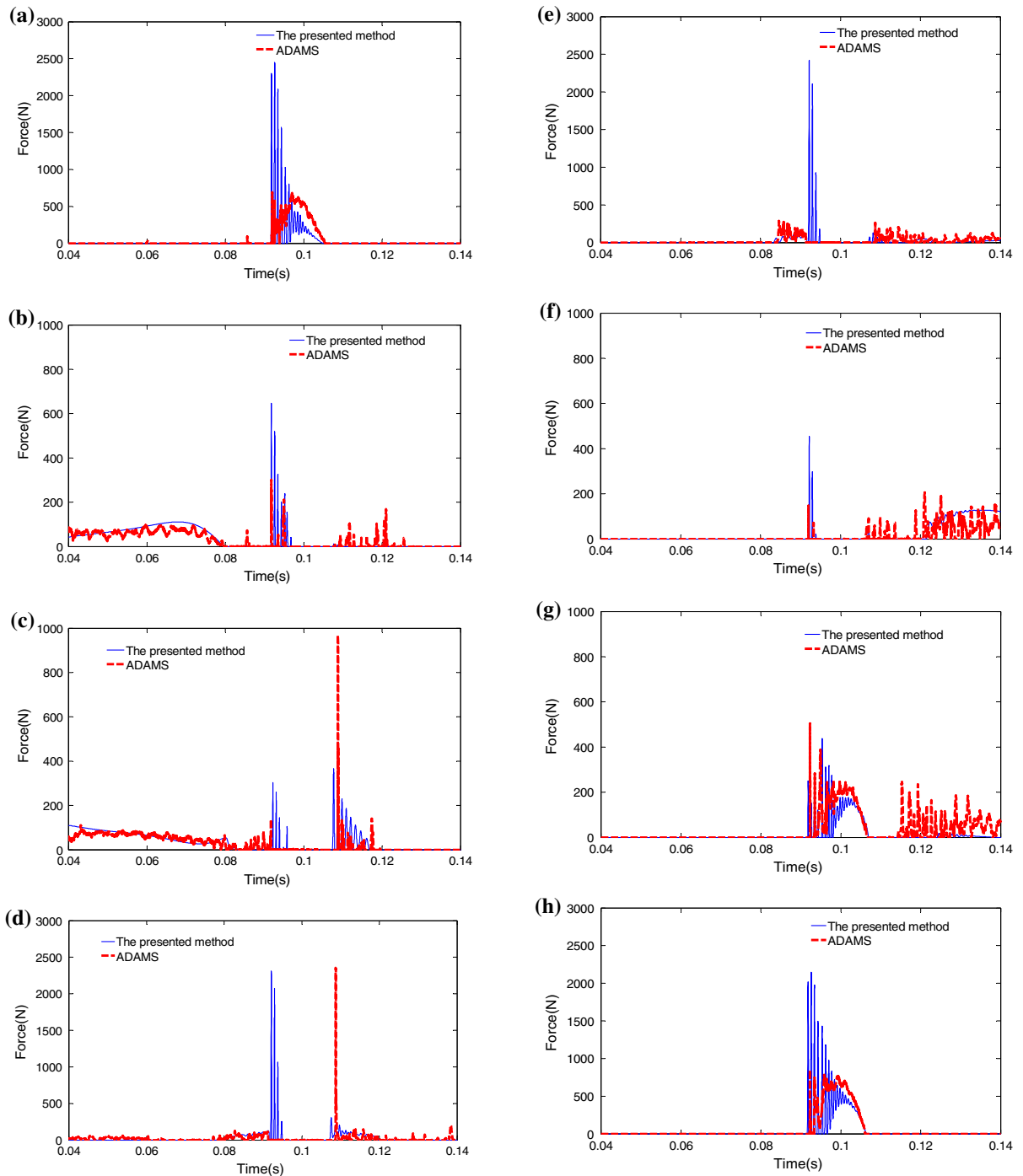


Fig. 20 Variations of the contact force on each rolling ball: **a** Ball 1, **b** Ball 2, **c** Ball 3, **d** Ball 4, **e** Ball 5, **f** Ball 6, **g** Ball 7, **h** Ball 8

rolling ball bearing joint and the dynamic load on each rolling ball. However, due to the influences of the radial clearance, the inertial load on the bearing, and the posi-

Fig. 20 continued

tion angles of the rolling balls, the load on the rolling balls of the bearing were governed by different relationships. Generally speaking, research into the fatigue lifetime and reliability of such bearings is based on the

analysis of the load characteristics. This study provided an effective method for the analysis of the distribution characteristics of dynamic load on rolling ball bearing joints under impact. Moreover, it offered support for the parameter optimisation of geometric structure, performance evaluation, and dynamic design of joints incorporating rolling ball bearings.

In addition, comparison with the ADAMS simulation model suggested that the theoretical method proposed in this study showed higher model solution efficiency and was more readily convergent. However, it failed to reveal the influences of external impact of the system on the dynamic response characteristics of the cage in the bearing. This was attributed to the fact that, in the theoretical method proposed in this study, the revolutions of the rolling balls in the bearing were controlled by kinematic constraints. In comparison, the ADAMS simulation model involved the real geometric structural characteristics of the inner and outer races, rolling balls, the cage of the bearing, and all corresponding complex dynamic contacts. Unfortunately, it was prone errors in the accuracy of its descriptions of complex three-dimensional curved surfaces. Since small fluctuations in size would result in large reaction forces in the contact, the stability of the simulation calculation was thereby difficult to guarantee. Moreover, there were complex multi-point contacts in the rolling ball bearing. The more numerous the contact points, the higher the contact stiffness, and the more difficult the ADAMS simulation.

It should be noted that both rolling, and sliding, friction at the ball bearing and in the contact between the slider and the target rigid body were neglected in this simulation. However, friction is an inevitable phenomenon and is one of the major limitations preventing good performance (both actual and simulated) in controlled mechanical systems, and hence it should be taken into account in the early stages of engineering design. In future research, the focus will be on the modelling of the impact of a multi-body system containing a bearing joint with friction.

Acknowledgments The authors would like to express the sincere thanks to the referees for their valuable suggestions. This project is supported by National Natural Science Foundation of China (Grant No. 51305300), Natural Science Foundation of Tianjin (Grant No. 13JCQNJC04500) and National Basic Research Program of China (973 Program, Grant No. 2013CB035403). These supports are gracefully acknowledged.

References

1. Zhen, Z., Liu, C.S.: The analysis and simulation for three-dimensional impact with friction. *Multibody Syst. Dyn.* **18**(4), 511–530 (2007)
2. Najafabadi, S.A.M., Kövecses, J., Angeles, J.: Impacts in multibody systems: modeling and experiments. *Multibody Syst. Dyn.* **20**(2), 163–176 (2008)
3. Bhalariao, K.D., Anderson, K.S.: Modeling intermittent contact for flexible multibody systems. *Nonlinear Dyn.* **60**(1–2), 63–79 (2010)
4. Flickinger, D.M., Bowling, A.: Simultaneous oblique impacts and contacts in multibody systems with friction. *Multibody Syst. Dyn.* **23**(3), 249–261 (2010)
5. Flores, P., Machado, M., Silva, M.T., Martins, J.M.: On the continuous contact force models for soft materials in multibody dynamics. *Multibody Syst. Dyn.* **25**(3), 357–375 (2011)
6. Rodriguez, A., Bowling, A.: Solution to indeterminate multipoint impact with frictional contact using constraints. *Multibody Syst. Dyn.* **28**(4), 313–330 (2012)
7. Flores, P., Leine, R., Glocker, C.: Application of the non-smooth dynamics approach to model and analysis of the contact-impact events in cam-follower systems. *Nonlinear Dyn.* **69**(4), 2117–2133 (2012)
8. Flores, P., Ambrósio, J.: On the contact detection for contact-impact analysis in multibody systems. *Multibody Syst. Dyn.* **24**(1), 103–122 (2010)
9. Lopes, D.S., Silva, M.T., Ambrósio, J.A., Flores, P.: A mathematical framework for rigid contact detection between quadric and superquadric surfaces. *Multibody Syst. Dyn.* **24**(3), 255–280 (2010)
10. Dopico, D., Luaces, A., Gonzalez, M., Cuadrado, J.: Dealing with multiple contacts in a human-in-the-loop application. *Multibody Syst. Dyn.* **25**(2), 167–183 (2011)
11. Machado, M., Moreira, P., Flores, P., Lankarani, H.M.: Compliant contact force models in multibody dynamics: evolution of the Hertz contact theory. *Mech. Mach. Theory* **53**, 99–121 (2012)
12. Khulief, Y.A.: Modeling of impact in multibody systems: an overview. *J. Comput. Nonlinear Dyn.* **8**(2), 0210121–02101215 (2012)
13. Ravn, P.: A continuous analysis method for planar multibody systems with joint clearance. *Multibody Syst. Dyn.* **2**(1), 1–24 (1998)
14. Flores, P., Ambrósio, J., Claro, J.C.P., Lankarani, H.M.: Dynamic behavior of planar rigid multi-body systems including revolute joints with clearance. *Proc. Inst. Mech. Eng. Part K* **221**(2), 161–174 (2007)
15. Koshy, C.S., Flores, P., Lankarani, H.M.: Study of the effect of contact force model on the dynamic response of mechanical systems with dry clearance joints: computational and experimental approaches. *Nonlinear Dyn.* **73**(1–2), 325–338 (2013)
16. Ravn, P., Shivaswamy, S., Alshaer, B.J., Lankarani, H.M.: Joint clearances with lubricated long bearings in multibody mechanical systems. *J. Mech. Design* **122**(4), 484–488 (2000)

17. Schwab, A.L., Meijaard, J.P., Meijers, P.: A comparison of revolute joint clearance models in the dynamic analysis of rigid and elastic mechanical systems. *Mech. Mach. Theory* **37**(9), 895–913 (2002)
18. Flores, P., Ambrósio, J., Claro, J.C.P.: Dynamic analysis for planar multibody mechanical systems with lubricated joints. *Multibody Syst. Dyn.* **12**(1), 47–74 (2004)
19. Flores, P., Lankarani, H.M., Ambrósio, J., Claro, J.C.P.: Modelling lubricated revolute joints in multibody mechanical systems. *Proc. Inst. Mech. Eng. Part K* **218**(4), 183–190 (2004)
20. Flores, P., Ambrósio, J., Claro, J.C.P., Lankarani, H.M., Koshy, C.S.: A study on dynamics of mechanical systems including joints with clearance and lubrication. *Mech. Mach. Theory* **41**(3), 247–261 (2006)
21. Alshaer, B.J., Nagarajan, H., Beheshti, H.K., Lankarani, H.M., Shivaswamy, S.: Dynamics of a multibody mechanical system with lubricated long journal bearings. *J. Mech. Design* **127**, 493–498 (2005)
22. Flores, P., Ambrósio, J., Claro, J.C.P., Lankarani, H.M., Koshy, C.S.: Lubricated revolute joints in rigid multibody systems. *Nonlinear Dyn.* **56**(3), 277–295 (2009)
23. Machado, M., Costa, J., Seabra, P., Flores, P.: The effect of the lubricated revolute joint parameters and hydrodynamic force models on the dynamic response of planar multibody systems. *Nonlinear Dyn.* **69**(1–2), 635–654 (2012)
24. Tian, Q., Zhang, Y.Q., Chen, L.P., (James) Yang, J.Z.: Simulation of planar flexible multibody systems with clearance and lubricated revolute joints. *Nonlinear Dyn.* **60**(4), 489–511 (2010)
25. Erkaya, S., Uzmay, I.: Investigation on effect of joint clearance on dynamics of four-bar mechanism. *Nonlinear Dyn.* **58**(1–2), 179–198 (2009)
26. Flores, P.: A parametric study on the dynamic response of planar multibody systems with multiple clearance joints. *Nonlinear Dyn.* **61**(4), 633–653 (2010)
27. Flores, P., Lankarani, H.M.: Dynamic response of multibody systems with multiple clearance joints. *J. Comput. Nonlinear Dyn.* **7**(3), 0310031–03100313 (2012)
28. Liu, C., Tian, Q., Hu, H.Y.: Dynamics and control of a spatial rigid-flexible multibody system with multiple cylindrical clearance joints. *Mech Mach. Theory* **52**, 106–129 (2012)
29. Megahed, S.M., Haroun, A.F.: Analysis of the dynamic behavioral performance of mechanical systems with multiple clearance joints. *J. Comput. Nonlinear Dyn.* **7**(1), 0110021–01100211 (2012)
30. Muvengei, O., Kihui, J., Ikuu, B.: Numerical study of parametric effects on the dynamic response of planar multi-body systems with differently located frictionless revolute clearance joints. *Mech. Mach. Theory* **53**, 30–49 (2012)
31. Muvengei, O., Kihui, J., Ikuu, B.: Dynamic analysis of planar rigid-body mechanical systems with two-clearance revolute joints. *Nonlinear Dyn.* **73**(1–2), 259–273 (2013)
32. Erkaya, S.: Trajectory optimization of a walking mechanism having revolute joints with clearance using ANFIS approach. *Nonlinear Dyn.* **71**(1–2), 75–91 (2013)
33. Xu, L.X., Li, Y.G.: Investigation of joint clearance effects on the dynamic performance of a planar 2-DOF pick-and-place parallel manipulator. *Robotics Comput.-Integr. Manuf.* **30**(1), 62–73 (2014)
34. Brutti, C., Coglitore, G., Valentini, P.P.: Modeling 3D revolute joint with clearance and contact stiffness. *Nonlinear Dyn.* **66**(4), 531–548 (2011)
35. Erkaya, S., Uzmay, I.: Experimental investigation of joint clearance effects on the dynamics of a slider–crank mechanism. *Multibody Syst. Dyn.* **24**(1), 81–102 (2010)
36. Flores, P., Koshy, C.S., Lankarani, H.M., Ambrósio, J., Claro, J.C.P.: Numerical and experimental investigation on multibody systems with revolute clearance joints. *Nonlinear Dyn.* **65**(4), 383–398 (2011)
37. Tian, Q., Liu, C., Machado, M., Flores, P.: A new model for dry and lubricated cylindrical joints with clearance in spatial flexible multibody systems. *Nonlinear Dyn.* **64**(1–2), 25–47 (2011)
38. Flores, P., Ambrósio, J., Claro, J.C.P., Lankarani, H.M.: Dynamics of multibody systems with spherical clearance joints. *J. Comput. Nonlinear Dyn.* **1**(3), 240–248 (2006)
39. Flores, P., Lankarani, H.M.: Spatial rigid-multibody systems with lubricated spherical clearance joints: modeling and simulation. *Nonlinear Dyn.* **60**(1–2), 99–144 (2010)
40. Tian, Q., Zhang, Y.Q., Chen, L.P., Flores, P.: Dynamics of spatial flexible multibody systems with clearance and lubricated spherical joints. *Comput. Struct.* **87**(13–14), 913–929 (2009)
41. Flores, P., Ambrósio, J., Claro, J.C.P., Lankarani, H.M.: Translational joints with clearance in rigid multibody systems. *J. Comput. Nonlinear Dyn.* **3**(1), 0110071–01100710 (2008)
42. Jang, G., Jeong, S.W.: Stability analysis of a rotating system due to the effect of ball bearing waviness. *J. Tribol.* **125**(1), 91–101 (2003)
43. Jang, G., Jeong, S.W.: Nonlinear excitation model of ball bearing waviness in a rigid rotor supported by two or more ball bearings considering five degrees of freedom. *J. Tribol.* **124**(1), 82–90 (2004)
44. Jang, G., Jeong, S.W.: Vibration analysis of a rotating system due to the effect of ball bearing waviness. *J. Sound Vib.* **269**(3–5), 709–726 (2004)
45. Bai, C.Q., Xu, Q.Y.: Dynamic model of ball bearings with internal clearance and waviness. *J. Sound Vib.* **294**(1–2), 23–48 (2006)
46. Upadhyay, S.H., Harsha, S.P., Jain, S.C.: Analysis of nonlinear phenomena in high speed ball bearings due to radial clearance and unbalanced rotor effects. *J. Vib. Control* **16**(1), 65–88 (2010)
47. Patel, V.N., Tandon, N., Pandey, R.K.: A dynamic model for vibration studies of deep groove ball bearings considering single and multiple defects in races. *J. Tribol.* **132**(4), 0411011–04110110 (2010)
48. Patil, M.S., Mathew, J., Rajendrakumar, P.K., Desai, S.: A theoretical model to predict the effect of localized defect on vibrations associated with ball bearing. *Int. J. Mech. Sci.* **52**(9), 1193–1201 (2010)
49. Nakhaeinejad, M., Bryant, M.D.: Dynamic modeling of rolling element bearings with surface contact defects using bond graphs. *J. Tribol.* **133**(1), 0111021–01110212 (2011)
50. Kappaganthu, K., Nataraj, C.: Nonlinear modeling and analysis of a rolling element bearing with a clearance. *Commun. Nonlinear Sci. Numer. Simul.* **16**(10), 4134–4145 (2011)

51. Liu, J., Shao, Y.M., Lim, T.C.: Vibration analysis of ball bearings with a localized defect applying piecewise response function. *Mech. Mach. Theory* **56**, 156–169 (2012)
52. Kankar, P.K., Sharma, S.C., Harsha, S.P.: Vibration based performance prediction of ball bearings caused by localized defects. *Nonlinear Dyn.* **69**(3), 847–875 (2012)
53. Xu, L.X., Yang, Y.H., Li, Y.G., Li, C.N., Wang, S.Y.: Modeling and analysis of planar multibody systems containing deep groove ball bearing with clearance. *Mech. Mach. Theory* **56**, 69–88 (2012)
54. Xu, L.X., Li, Y.G.: An approach for calculating the dynamic load of deep groove ball bearing joints in planar multibody systems. *Nonlinear Dyn.* **70**(3), 2145–2161 (2012)
55. Harris, T.A., Kotzalas, M.N.: *Rolling Bearing Analysis*. Wiley, New York (2006)
56. Tiwari, M., Prakash, O., Gupta, K.: Effect of radial internal clearance of a ball bearing on the dynamics of a balanced, horizontal rotor. *J. Sound Vib.* **238**(5), 723–756 (2000)
57. Dietl, P., Wensing, J., van Nijen, G.C.: Rolling bearing damping for dynamic analysis of multi-body systems—experimental and theoretical results. *Proc. Inst. Mech. Eng. Part K* **214**(1), 33–43 (2000)
58. Mitsuya, Y., Sawai, H., Shimizu, M., Aono, Y.: Damping in vibration transfer through deep-groove ball bearings. *J. Tribol.* **120**(3), 413–420 (1998)
59. Hertz, H.: On the contact of solids—on the contact of rigid elastic solids and on hardness. *Miscellaneous papers 1896*, pp. 146–183. Macmillan, London (1896)
60. Zukas, J.A., Nicholas, T., Greszczuk, L.B., Curran, D.R.: *Impact Dynamics*. Wiley, New York (1982)
61. Lankarani, H.M., Nikraves, P.E.: A contact force model with hysteresis damping for impact analysis of multibody systems. *J. Mech. Design* **112**(3), 369–376 (1990)
62. Dubowsky, S., Freudenstein, F.: Dynamic analysis of mechanical systems with clearances, part I: formulation of dynamic model. *J. Eng. Ind. Ser. B* **93**(1), 305–309 (1971)
63. Johnson, K.L.: *Contact Mechanics*. Cambridge University Press, Cambridge (1994)
64. Radzimovsky, E.I.: Stress distribution and strength conditions of two rolling cylinders pressed together. University of Illinois. Engineering Experiment Station. Bulletin series 408 (1953)
65. Goldsmith, W.: *Impact: The Theory and Physical Behavior of Colliding Solids*. Edward Arnold, London (1960)
66. Flores, P., Ambrósio, J., Claro, J.C.P., Lankarani, H.M.: *Kinematics and Dynamics of Multibody Systems with Imperfect Joints*. Springer, Berlin (2008)
67. Minamoto, H., Kawamura, S.: Moderately high speed impact of two identical spheres. *Int. J. Impact Eng.* **38**(2–3), 123–129 (2011)
68. Dubowsky, S.: On predicting the dynamic effects of clearances in planar mechanisms. *J. Eng. Ind. Ser. B* **96**(1), 317–323 (1974)
69. Rooney, G.T., Deravi, P.: Coulomb friction in mechanism sliding joints. *Mech. Mach. Theory* **17**, 207–211 (1982)
70. Threlfall, D.C.: The inclusion of Coulomb friction in mechanisms programs with particular reference to DRAM. *Mech. Mach. Theory* **13**, 475–483 (1978)
71. Karnopp, D.: Computer simulation of stick-slip friction in mechanical dynamic systems. *J. Dyn. Syst. Meas. Control* **107**, 100–103 (1985)
72. Ambrósio, J.: Impact of rigid and flexible multibody systems: deformation description and contact models. *Virtual Nonlinear Multibody Syst. NATO ASI Ser.* **103**, 57–81 (2003)
73. Baumgarte, J.: Stabilization of constraints and integral of motion in dynamical systems. *Comput. Methods Appl. Mech. Eng.* **1**(1), 1–16 (1972)
74. Flores, P., Machado, M., Seabra, E., Silva, M.T.: A parametric study on the Baumgarte stabilization method for forward dynamics of constrained multibody systems. *ASME J. Comput. Nonlinear Dyn.* **6**(1), 011019 (2011)